Block-wise Motion Detection Using Compressive Imaging System

Jun Ke [a,*], Amit Ashok [a], Mark A. Neifeld [a,b]

[a] *Department of Electrical Computer Engineering, University of Arizona, Tucson, AZ 85721-0104, USA*

[b] *College of Optical Sciences, University of Arizona, Tucson, AZ 85721-0104, USA*

Abstract

A block-wise motion detection strategy based on compressive imaging, also referred to as feature-specific imaging (FSI), is described in this work. A mixture of Gaussian distributions is used to model the background in a scene. Motion is detected in individual object blocks using feature measurements. Gabor, Hadamard binary and random binary features are studied. Performance of motion detection methods using pixel-wise measurements is analyzed and serves as a baseline for comparison with motion detection techniques based on compressive imaging. ROC (Receiver Operation Characteristic) curves and AUC (Area Under Curve) metrics are used to quantify the algorithm performance. Because a FSI system yields a larger measurement SNR(Signal-to-Noise Ratio) than a traditional system, motion detection methods based on the FSI system have better performance. We show that motion detection algorithms using Hadamard and random binary features in a FSI system yields AUC values of 0.978 and 0.969 respectively. The pixel-based methods are only able to achieve a lower AUC value of 0.627.

Key words: Compressive imaging, Feature specific imaging, Motion Detection, Tracking, Gaussian Mixture Model

1 Introduction

Motion detection is an integral part of the object tracking problem. Object tracking has received widespread interest from several research communities over the years. It has broad applications spanning civilian, military, and scientific research domains. Examples include traffic control, security surveillance, bio-imaging, battle field monitoring, and sub-sea video processing [1, 2, 3, 4, 5, 6]. In radar signal processing, Ground Moving Target Indicator (GMTI) radar has proved to be a very successful example of object tracking [7, 8]. In computer vision, an object tracking problem is viewed as a two-part problem: motion prediction and object matching problem [3]. Kalman filter [9] and particle filter [10] are among the most popular algorithms devised for the motion prediction problem [11, 2, 5]. To solve the object matching problem many different strategies have been developed such as, extracting features, calculating optical flows [3, 5, 11, 2], using rigid shapes [3, 5, 11], and matching deformable contours [12, 13]. Besides the motion prediction and object matching, another critical step in object tracking problem involves motion detection, which typically entails modeling the background or clutter, then subtracting it from a frame in a video sequence to find the moving regions [14, 15, 5, 11, 16]. Note that solving the motion detection problem can be

* Corresponding author.
Email address: jke@ece.arizona.edu (Jun Ke).
[1] Present address: University of Arizona, Electrical Computer Engineering. 1230 E speedway Bldg 112, Tucson, AZ, 85721-0001, USA.

thought of as equivalent to solving the background subtraction problem. Proposed by Wren et al. [17], one of the earliest approaches that have been developed uses a single Gaussian distribution to model a static background at each pixel position. Subsequently, Grimson et al. developed a more sophisticated model that uses a mixture of Gaussian distribution to describe the individual pixel values in outdoor scenes [18]. In this model for motion detection, a pixel in the current frame is compared with the several Gaussian distributions to find a match. If the pixel measurement can not be matched to any distribution, it is classified as a foreground pixel and thus motion is detected. This method is fast and can be easily adjusted for clutter or illumination changes. To further extend this Gaussian mixture model, Elgammal et al. [19] used a non-parametric kernel density estimation to describe a pixel intensity. Other methods for background subtraction include incorporating region-based scene information instead of only using single pixel information and representing the intensity variation of a pixel in a video sequence as discrete states in Hidden Markov Models (HMM) [11, 16].

Note that nearly all the methods reviewed here are based on pixel level image measurements. It is common for a digital camera today to yield a multi-megapixel image. Therefore, the pixel-wise model approach can quickly become computationally expensive. In most cases, a moving object extends over multiple pixels, therefore the motion exits at a group of adjoining pixel positions. To detect motion in a region we can not assume pixel-wise motion detection strategy is the best approach. In this work, we discuss a strategy to detect motion in a region directly. A region is defined as an object block. After discussing motion detection in object block space and its corresponding feature space, we introduce a system which makes measurements directly in the feature space. This measurement scheme is *compressive* as the number of measurements, each measurement corresponds to one feature, is typically much smaller than the dimensionality of the object block. Such a system is referred to as a feature-specific imaging (FSI) system or compressive imaging system in some research community. The paper is organized as follows: in section 2, motion detection methods with pixel-wise measurements are discussed. We first introduce the Gaussian mixture model for individual pixels. Then the model is extended to a block-wise mixture model for an object block and a corresponding mixture model in the feature space of each block. In section 3, simulation results for the detection methods described in section 2 are presented. In section 4, we define the FSI system using the parallel optical architecture followed by a description of motion detection algorithms designed for FSI measurements. In section 5, we present the simulation results for the motion detection methods using FSI system. Finally, in section 6 we draw conclusions based on the results of our simulation study.

2 Motion Detection with Pixel-wise Measurement

2.1 Pixel-wise motion detection using Gaussian mixture model

The intensity history for a pixel from time 0 to time t can be represented as a vector $\mathbf{x}_t = [x(0)\ x(1)\ ...\ x(t)]^T$ as shown in figure 1 a). Here, we model this vector as a random vector drawn from a mixture of Gaussian distributions [18, 20]. Using K distributions, the probability density function (pdf) of $\mathbf{x}_t$

can be expressed as

$$p(\mathbf{x}_t) = \sum_{i=1}^{K} w_{i,t} * p(\mathbf{x}_t, \mu_{i,t}, \Sigma_{i,t}) \ \text{ with } \ \sum_{i=1}^{K} w_{i,t} = 1, \tag{1}$$

where $w_{i,t}$, $\mu_{i,t}$, and $\Sigma_{i,t}$ are the estimates of the weight, the mean value vector, and the covariance matrix of the i^{th} Gaussian in the mixture, respectively. The ith Gaussian pdf $p(\mathbf{x}_t, \mu_{i,t}, \Sigma_{i,t})$ is defined as

$$p(\mathbf{x}_t, \mu_{i,t}, \Sigma_{i,t}) = \frac{1}{(2\pi)^{\frac{n}{2}} |\Sigma_{i,t}|^{\frac{1}{2}}} e^{-\frac{1}{2}(\mathbf{x}_t - \mu_{i,t})^T \Sigma_{i,t}^{-1} (\mathbf{x}_t - \mu_{i,t})}, \tag{2}$$

where $\Sigma_{i,t}$ is assumed to be $\Sigma_{i,t} = \sigma_{i,t}^2 \mathbf{I}$ [18]. The K components in equation (1) are sorted in descending order based on $\frac{w_{i,t}}{\sigma_{i,t}}$ such that $\frac{w_{1,t}}{\sigma_{1,t}} \geq \frac{w_{2,t}}{\sigma_{2,t}} \geq \cdots \geq \frac{w_{K,t}}{\sigma_{K,t}}$. The weight to standard deviation ratio $\frac{w_{i,t}}{\sigma_{i,t}}$ is a reasonable parameter to sort the components, because $w_{i,t}$ represents the contribution of the i^{th} pdf to the mixture and variance estimate $\sigma_{i,t}$ represents the uncertainty of the contribution. Using equation (1), we can determine if a new pixel measurement belongs to the current model. For example, we use the criteria that: at time $t+1$, $\mathbf{x}_{t+1} = [x(1)\ x(2)\ ...\ x(t+1)]^T$ belongs to the model if it is within 2.5 standard deviations of the mean value of any of the K Gaussian distributions.

The K distributions are divided into two groups of size B and $K - B$. The first B distributions in equation (1) (i.e., those with the largest $\frac{w_{i,t}}{\sigma_{i,t}}$ values) define a mixture model for a pixel without motion which defines a background pixel. A pixel at a position with motion is called a foreground pixel. For a new pixel measurement at time $t+1$, if $\mathbf{x}_{t+1}$ matches with any of the first B distributions, the pixel is a background pixel, otherwise a foreground pixel. B is defined as

$$B = \min_b \left(\sum_{i=1}^{b} w_{i,t} > W\right), \tag{3}$$

where W is a pre-defined threshold. Because the distributions in equation (1) are sorted in descending order based on $\frac{w_{i,t}}{\sigma_{i,t}}$, the first B distributions have the largest $\frac{w_{i,t}}{\sigma_{i,t}}$ values. When measurements at one pixel position in several frames belongs to one Gaussian distribution, the weight parameter $w_{i,t}$ is large. A small $\sigma_{i,t}$ means the measurements belong to the distribution with high certainty. Therefore the first B distributions form a model for a background pixel, or a pixel with stable measurements. Note that the last $K-B$ distributions are affected by pixel measurements from last few frames. These measurements represent foreground pixels which might progressively represent background later.

After motion detection at time t, the measurement $\mathbf{x}_{t+1}$ is used to update the mixture model in equation (1) with following online expectation maximization (EM) algorithm [20]:

$$(1)\ \ \hat{d}(w_{i,t}|\mathbf{x}_{t+1}) = \begin{cases} 1; & \text{if the } i^{th} \text{ Gaussian is the first distribution which } \mathbf{x}_{t+1} \text{ belongs to} \\ 0; & \text{otherwise} \end{cases}$$

$$(2)\ \ \hat{w}_{i,t+1} = \hat{w}_{i,t} + \alpha \ \left(\ \hat{d}(w_{i,t}|\mathbf{x}_{t+1}) - \hat{w}_{i,t} \ \right)$$

$$(3)\ \ \hat{\mu}_{i,t+1} = \hat{\mu}_{i,t} + \alpha \ (\ \frac{\hat{d}(w_{i,t}|\mathbf{x}_{t+1}) \ \mathbf{x}_{t+1}}{\hat{w}_{i,t+1}} - \hat{\mu}_{i,t} \ )$$

$$(4)\ \ \hat{\mathbf{\Sigma}}_{i,t+1} = \hat{\mathbf{\Sigma}}_{i,t} + \alpha \ (\ \frac{\hat{d}(w_{i,t}|\mathbf{x}_{t+1}) \ \triangle\hat{\mathbf{\Sigma}}_{i,t}}{\hat{w}_{i,t+1}} - \hat{\mathbf{\Sigma}}_{i,t} \ )$$

where α is an positive update parameter much smaller than 1, and $\triangle\hat{\mathbf{\Sigma}}_{i,t}$ is a diagonal matrix which has same diagonal elements as the matrix $(\mathbf{x}_{t+1} - \hat{\mu}_{i,t})(\mathbf{x}_{t+1} - \hat{\mu}_{i,t})^T$. Note that $\hat{w}_{i,t+1}$, $\hat{\mu}_{i,t+1}$, and $\hat{\mathbf{\Sigma}}_{i,t+1}$ can be rewritten as follows:

- $\hat{w}_{i,t+1} = (1-\alpha) \ \hat{w}_{i,t} + \alpha \ \hat{d}(w_{i,t}|\mathbf{x}_{t+1})$
- $\hat{\mu}_{i,t+1} = (1-\alpha) \ \hat{\mu}_{i,t} + \alpha \ \frac{\hat{d}(w_{i,t}|\mathbf{x}_{t+1}) \ \mathbf{x}_{t+1}}{\hat{w}_{i,t+1}}$
- $\hat{\mathbf{\Sigma}}_{i,t+1} = (1-\alpha) \ \hat{\mathbf{\Sigma}}_{i,t} + \alpha \ \frac{\hat{d}(w_{i,t}|\mathbf{x}_{t+1}) \ \triangle\hat{\mathbf{\Sigma}}_{i,t}}{\hat{w}_{i,t+1}}$

The parameter α is positive and $w_{i,t}$ is between 0 and 1, therefore observe that the estimate of $\hat{w}_{i,t+1}$, $\hat{\mu}_{i,t+1}$, and $\hat{\mathbf{\Sigma}}_{i,t+1}$ will be positive after each update. If $\mathbf{x}_{t+1}$ matches none of the K distributions, the last distribution in the model is replaced by a new Gaussian distribution with $\mathbf{x}_{t+1}$ as its mean and an initially high variance and low prior weight in equation (1).

We refer to this Gaussian mixture model as the pixel-wise Gaussian mixture model. Foreground pixel detection is applied to each pixel position in a frame which also involves updating the mixture model for each pixel. Therefore, this pixel-wise motion detection method is computationally intensive. The memory and computational cost for the method are $O(KNt^2)$ and $O(KNt)$ respectively when there are N pixels in the object scene. As discussed in introduction section, motion detection at each pixel is often used to search for a moving object. Finite moving object size suggests that detecting motion in an object block or a region over the whole object scene as opposed to doing it pixel-wise may be more appropriate. To solve this motion detection problem for an object block, we extend the pixel-wise Gaussian mixture model to a block-wise mixture model.

2.2 Block-wise motion detection using Gaussian mixture model

As shown in figure 1 b), pixel values within a block of size $\sqrt{N} \times \sqrt{N}$***, at time*** t***, are rearranged into a vector*** $\mathbf{x}_b(t)$ ***of size*** $(N \times 1)$***.*** The block pixels intensity history from time 0 to L is represented as $\mathbf{x}_{bL} = [\mathbf{x}_b^T(0)\ \mathbf{x}_b^T(1)\ ...\ \mathbf{x}_b^T(L)]^T$. To simplify notation, $\mathbf{x}_{bL}$ will be written simply as $\mathbf{x}$. Note that the pixel-wise measurement vector $\mathbf{x}_t$ consists of data points along a line in figure 1 a), while the measurement vector $\mathbf{x}$ consists of data points in a cube in figure 1 b). Once again we model $\mathbf{x}$ as a mixture of Gaussian distributions similar to the model used for $\mathbf{x}_t$. We refer to this model as a block-wise Gaussian mixture model. Using the same procedure as the one described in last subsection, a block vector measurement matching with any of the most significant B Gaussian components in the model, is classified as a background block, otherwise it is declared as a foreground block. After making the motion detection decision, the block-wise Gaussian mixture model is updated with the new block measurements.

The block-wise motion detection method uses information jointly among neighboring pixels. Therefore, its theoretical performance should be no worse than the pixel-wise motion detection method. However, both detection strategies involve processing all pixels directly for updating the mixture models and making detection decisions. Also note that the decision for motion detection is binary. Therefore, we believe there is inherent redundancy in the measurement data for the binary decision problem. This motivates our compressive method in the following subsection, where the measurement vector $\mathbf{x}$ is compressed into a lower dimensional feature space before making motion detection decision.

2.3 Feature-space motion detection using Gaussian mixture model

A feature of an object is defined as the inner product between an object $\mathbf{x}$ and a projection vector from the feature basis. It can be represented as $\mathbf{y} = \mathbf{F}\mathbf{x}$, where $\mathbf{y}$ is the feature vector of size $(M \times 1)$, $\mathbf{F}$ is the projection matrix of size $M \times NL$, and $\mathbf{x}$ is the object vector of size $NL \times 1$. With detector noise $\mathbf{n}$, of size $N \times 1$ considered, feature representation is modified as $\mathbf{y} = \mathbf{F}(\mathbf{x} + \mathbf{n})$. Here, we will consider 2D-Gabor [21], Hadamard binary, and random binary features for the motion detection task. Figure 2 shows examples of the types of projections. Gabor and Hadamard projections are widely used in image processing, object detection and pattern recognition applications [22, 23, 24, 25, 26, 27, 28]. We consider binary non-negative Hadamard projection in this paper. Random projection has become popular in compressive sensing and machine learning field [29, 30]. We use binary non-negative random projections to ensure a fair comparison with binary non-negative Hadamard projections. Once again a Gaussian mixture model is used to detect motion in feature space.

Note that the choice of a particular feature is key in determining the motion detection algorithm performance. Therefore, features need to be sorted to optimize the algorithm performance and achieve the best performance with the least number of features. A divergence based feature selection method is used for sorting features [31]. In this method, a feature vector belongs to one of the two classes, class ω_1 and class ω_2 for blocks with and without motion, respectively. In each class, a feature vector is modeled as a random vector with a parametric model [31] constructed using training data. With this model, Kullback J-divergence between classes ω_1 and ω_2 can be measured and used to sort features. The J-divergence, is defined as

$$J(\omega_1, \omega_2) = E_{\mathbf{y}|\omega_1}\{log\, \frac{p(\mathbf{y}|\omega_1)}{p(\mathbf{y}|\omega_2)}\} + E_{\mathbf{y}|\omega_2}\{log\, \frac{p(\mathbf{y}|\omega_2)}{p(\mathbf{y}|\omega_1)}\}, \tag{4}$$

where $E_{\mathbf{y}|\omega_i}$ denotes the mathematical expectation with respect to the class-conditional PDF $p(\mathbf{y}|\omega_i)$ with $i = 1$, or 2. Observe that if the two classes are well separated, then $\frac{p(\mathbf{y}|\omega_2)}{p(\mathbf{y}|\omega_1)}$ or $\frac{p(\mathbf{y}|\omega_1)}{p(\mathbf{y}|\omega_2)}$ is large, resulting in a higher $J(\omega_1, \omega_2)$ value. J-divergence [31], $J(\omega_1, \omega_2)$ can be decomposed into independent components attributed to different features. Using an EM algorithm described in [31], the independent J-divergence components are computed, then the most significant M features are selected for motion detection.

3 Motion Detection Performance Using Pixel-wise Measurements

A video clip with a hundred frames taken from the CAVIAR [32] database is used in the simulation study here. The video is filmed in the entrance lobby of the INRIA Labs at Grenoble, France. Each frame has size 288×384 with dynamic range $[0, 255]$. Figure 3 shows two example frames. To generate the ground truth, video frames are labeled by isolating the foreground and background regions manually. The object block size is chosen as 32×32 in this section. Four different noise levels $\sigma_0 = 0,\ 20,\ 100,\ 200$ are considered. The acronyms for the motion detection algorithms studied in this section are defined as follows:

(1) CP (Conventional measurement with Pixel-wise mixture model) algorithm: In this algorithm, Gaussian mixture model is employed for each pixel and foreground pixels are detected at individual pixel position. A block is decided as a moving block if there are κ foreground pixels detected within the block, where κ is a predefined integer between 1 and NL.

(2) CB (Conventional measurement with Block-wise mixture model) algorithm: In this algorithm, moving object block is detected using block-wise Gaussian mixture model.

(3) CDB (Conventional measurement with mixture model using Block Difference) algorithm: In this algorithm, Gaussian mixture model is formulated for the difference between object blocks in two consecutive frames. The difference is used for motion detection in each block.

(4) CFG, CFHB, or CFRB (Conventional measurement with mixture model using Gabor, Hadamard-Binary, or Random Binary feature) algorithm: In this algorithm, a Gaussian mixture model is formulated in feature space using Gabor, Hadamard binary, and random binary features. Features are used for block motion detection.

To evaluate algorithm performance, we employ the ROC (Receiver Operating Characteristic) and the AUC (Area Under Curve) metrics. The x and y axes in a ROC curve are the false positive rate(FPR) and the true positive rate(TPR) respectively. FPR is defined as the probability of motion detection when there is actually no motion, while TPR is defined as the probability of motion detection when motion is present. Based on the ground truth generated manually, a block with one or more than one foreground pixels is defined as a moving block. In each ROC curve, the largest TPR value is generated for a fixed FPR by searching the parameter space spanned by L, $\Sigma_{i,0}$, and W variables in the motion detection algorithm. In CP algorithm, the threshold number of foreground pixels in each block, κ, is also optimized. The optimal values are used in all data presented here. The AUC value is calculated by integrating the area under the ROC curve.

Table 1 lists the AUC values using the algorithms discussed with noiseless measurement. In CFG, CFHB, and CFRB algorithms, $M = 1$ feature is used for motion detection. It can be observed from table 1 that all algorithms have detection performance close to 1, where 1 indicates perfect performance. Therefore, we conclude that $M = 1$ noiseless feature is sufficient for detecting motion when the object block has dimension 1024 (32×32). Note that, the computation cost for CFG, CFHB, and CFRB algorithms is also reduced due to using the Gaussian mixture model in feature space. The amount of memory and computation steps required are $O(KML^2)$ and $O(KML)$ respectively, where $M \ll N$.

Figure 4 a), b), and c) shows the ROC curves for all algorithms at noise level $\sigma_0 = 20,\ 100,$ and 200 respectively. It is observed that CP algorithm has better performance than CB and CDB algorithms at all noise levels. In CDB algorithm, the consecutive frame feature measurements are subtracted from each other, therefore the noise is twice as much as it is in other algorithms. Therefore, CDB algorithm has the worst performance when noise is high as $\sigma_0 = 100,$ or 200. As discussed earlier, ideally CB algorithm should have no worse performance as CP algorithm. However, the data dimensionality of the observation vector in CB algorithm is much higher than CP algorithm, therefore estimation of the parameters such as $\mathbf{\Sigma}$ and μ require more samples. Figure 5 shows the ROC curves for CP and CB algorithm when noise level $\sigma_0 = 100$ and object block size is 4×4 and 32×32. It can be observed when the object block size is small, the CB algorithm has superior performance compared to the CP algorithm.

Among the algorithms using features for motion detection, the CFG algorithm has the worst performance. From figure 2 we can observe that most Gabor projection vector elements have values close to 0. Therefore, using Gabor projection, limited signal power is collected in each feature. In feature space, signal to noise ratio using Gabor projection is smaller compared to using Hadamard and random binary projections. Also note that CFHB and CFRB algorithms have similar performance. Figure 6 a) and b) show two projection vectors used in CFHB and CFRB algorithms. The Hadamard projection vector does not have significant spatial variation over a block. On the other hand, the random projection vector has a lot of variation over the 32×32 object block area. Therefore, we expect that the random vector would be superior to the Hadamard vector as a result of increased sensitivity to fine motion details. However, the motion in the experiment video used in our study occurs mainly on a large scale as shown in figure 6 c) and d). Therefore, in our case both algorithms yield similar performances.

It is also observed that when noise is high such as $\sigma_0 = 100$ and 200, detection algorithms employing Hadamard and random binary features achieve a superior motion detection performance relative to CP, and CB algorithms. We compare the measurement SNR in CFHB and CP algorithms as a representative example to explain this observation. In the CP algorithm, the signal power is $S_{CP} = E\{||\mathbf{x}||^2\} = E\{\sum_{i=1}^{NL} x_i^2\}$, where x_i is the object pixel value in L consecutive object blocks with $1 \le i \le NL$. The noise power is $\varepsilon_{CP} = NL\sigma_0^2$ as the detector noise is assumed to be independent from each other. In CFHB algorithm, the feature value is defined as $\sum_{i=1}^{NL}[f_i(x_i + n_i)]$. Signal power is written as $E\{(\sum_{i=1}^{NL} f_i x_i)^2\}$. Because any Hadmard binary projection has half elements zeros and the other half ones, the signal power can be reformulated as $S_{CFHB} = 0.5 \times E\{\sum_{i=1}^{NL} x_i^2\} + E\{\sum_{i,j=1;\, i\neq j}^{NL} f_i f_j x_i x_j\} = 0.5 \times S_{CP} + E\{\sum_{i,j=1;\, i\neq j}^{NL} f_i f_j x_i x_j\}$. Notice the second term in S_{CFHB} is strictly non-negative. Using the same derivation it can be found out that the noise power in CFHB algorithm is $\varepsilon_{CFHB} = 0.5 \times NL\sigma_0^2 = 0.5 \times \varepsilon_{CP}$. Putting the signal and noise power values together, it is clear that the SNR value in CFHB is larger than it in CP algorithm. Hence CFHB algorithm has better performance. Note that this performance improvement for CFHB due to SNR advantage is more significant when detector noise σ_0 is larger. To further improve motion detection method performance, the measurement SNR needs to be increased. Note that using pixel-wise measurements to calculate a feature value includes noise from NL detectors in each feature value. By employing a FSI system, features can be measured directly. This implies that each feature measurement includes noise only at one detector. This motivates us to study FSI system [33, 34, 35] performance for the motion detection task.

4 Motion Detection with Feature-specific Imaging System

To directly measure features in a FSI system, an electro-optic modulation device is employed. Examples of such electro-optic modulation device include a spatial light modulator (SLM) such as liquid crystal panel and digital micro-mirror device (DMD). A FSI system has several advantages over a conventional imaging system including fewer number of detectors, simpler hardware, lower cost, and higher measurement SNR [33, 36]. A FSI system can be implemented via three distinct optical systems: sequential, parallel, and pipeline architectures [34]. In a sequential architecture, the measurements are acquired sequentially one after the other. The measurements in parallel and pipeline architectures are taken simultaneously or in one snapshot. Among the three architectures, pipeline architecture presents the best photon efficiency, but incurs the highest system complexity. Relatively, the parallel architecture has superior photon collecting efficiency compared to sequential architecture and retains a simple structure. Therefore, in this paper, the parallel architecture is considered in the simulation study. Figure 7 shows an example FSI system employing the parallel architecture via a lenslet array. In such a system, the aperture contains a lenslet array with M elements of equal size. Following each sub-aperture, a simple mask together with a detector is used to measure one feature. Note that as the measured object illumination is proportional to the sub-aperture area, signal intensity at each detector is $\frac{1}{M}$ of the original object total intensity. Detector noise is once again modeled as independent white Gaussian noise with standard deviation σ_0. Feature measurements using the parallel architecture FSI system are therefore mathematically defined as $\mathbf{y} = \frac{1}{M}\mathbf{F}\mathbf{x} + \mathbf{n}$.

To detect motion in blocks, we employ the same Gaussian mixture model as the one used in CB. Note that in the FSI system, there is only one detector noise component per feature measurement. Therefore, the noise power in all motion detection methods using FSI measurements is σ_0^2, which much smaller than $NL\sigma_0^2$ and $0.5 \times NL\sigma_0^2$ in CP and CFHB algorithms respectively. Therefore, we expect that by using FSI it is possible to achieve significant improvements in motion detection algorithm performance.

5 Motion Detection Performance Using Direct Feature Measurements

The FSI-based motion detection algorithms using Gabor, Hadamard, and random binary features are denoted by FG, FHB, and FRB respectively. Figure 8 shows the ROC curves for the three algorithms using $M = 1$ feature for three detector noise levels $\sigma_0 = 20,\ 100,$ and 200. Features are chosen according to the J-divergence based feature selection method discussed in section 2. The results for CP, CFG, CFHB, and CFRB algorithms are also presented for comparison. There are several observations that can be made from this figure. The first observation is that FSI-based motion detection algorithms FG, FHB, and FRB have significantly higher performance compared with the CFG, CFHB, and CFRB algorithms, respectively. For example, when FPR has value 0.1 and noise level is $\sigma_0 = 20$, CFG, CFHB, and CFRB algorithms have TPR of 0.27, 0.93, and 0.91 respectively, while FG, FHB, and FRB algorithms have TPR of 0.83, 0.95, and 0.99, respectively. As the measurement SNR in FSI system is much higher than a conventional system, the motion detection algorithms using FSI system achieve better performance. The second observation is that FHB and FRB algorithms perform much better than FG algorithm. When FPR value is 0.1 with the noise level $\sigma_0 = 200$, the TPR values for FG, FHB, and FRB algorithms are 0.12, 0.96, and 0.94 respectively. As the Gabor projection vector has more than half elements with a value close to zero, the object energy collected in feature measurement is smaller than the energy collected in the Hadamard and random feature values. Comparing Hadamard binary and random binary projections, the performances for FHB and FRB algorithms are very similar. The third observation is that CP algorithm has better performance than FG algorithm, but much worse than FHB and FRB methods, especially at high noise levels. From this observation, we conclude that not all features in FSI system are superior to the conventional pixel-wise measurements for motion detection especially for low measurement SNR.

As shown in figure 9, FG algorithm has clearly worse motion detection performance through all three noise levels using $M = 4$ ***compared with*** $M = 1$ ***features. The same trend can be observed for the FHB and FRB algorithms with noise levels*** $\sigma_0 = 100$***, and 200. This is due to the fact that the measured signal power is reduced by factor of four when*** $M = 4$ ***features are collected in the parallel architecture FSI system. As a result, the algorithm performance suffers from smaller measurement SNR. It is also important to em-***

phasize that the projection vectors used in these algorithms are not ordered/sorted according to their corresponding feature energy. Instead, as discussed in previous section, the projection vectors are sorted based on the J-divergence distance between blocks with and without motion in a feature subspace spanned by these vectors. Figure 10 shows the first 4 vectors of Gabor, Hadamard binary, and random binary projections used in the simulation study ordered (from left to right, left with the highest metric value) according to our task-optimal metric. Accordingly, here we note that first Hadamard binary projection vector is not the all-one vector which would correspond to highest feature energy. For the purpose of projection vector sorting we have utilized a set of training frames, however, a different set of frames are used for testing and quantifying motion detection performance to ensure that our results are robust.

Figure 11 a) & b) show the ROC curves for FHB, and FRB algorithms using 1 feature measurement with different block size and two noise levels. Object block with size 8×8, 16×16, 32×32, and 48×64 are considered. The noise levels are $\sigma_0 = 20$ and 200. From both figures, it can be observed that increasing the block size improves the performance, as a result of increasing measurement SNR. The other observation is that system performance in FHB and FRB algorithms do not degrade significantly when noise level increases from $\sigma_0 = 20$ to $\sigma_0 = 200$. Thus, both the algorithms have robust performance with increasing detector noise. This observation can also be supported by AUC values for different detection algorithms as shown in figure 12 and table 2.

So far all results presented was on a training data set. To validate the performance of the various algorithms, we now consider a test data set which is distinct from the training data set. Figure 13 presents a set of frames using CFHB and FHB algorithms. The area which has positive response for motion detection is indicated with higher intensity. The scene in this sequence of video frames is a car moving towards a building. Note that the tree leaves shaking due to wind are not a target of interest. As such, we consider them as clutter and would like then to be classified as background. The covariance matrix $\mathbf{\Sigma}_{i,t}$ in the mixture model is assigned with large initial values to include the potentially moving clutter in background. From figure 13 it is clear that using the FHB algorithm the false alarm area is much smaller than using the CFHB algorithm. This demonstrates that motion detection using FSI system also works for scenes with clutter.

6 Conclusion

In this paper, we use the Gaussian mixture model developed by Grimson et al. [18] for block-wise motion detection. With pixel-wise measurements, several motion detection algorithms, CP, CB, CDB, CFG, CFHB, and CFRB, are studied. The CP algorithm is used as a baseline throughout the study. The Gaussian mixture model was extended to a block-wise mixture model, and the CB and CDB methods were considered. Then feature calculated from pixel values were considered for motion detection. It was observed that as a result of improved SNR in case of in CFHB and CFRB algorithms, they achieved larger AUC values than CP and CB algorithms, especially when detector noise is high. For example, compared with the AUC value 0.6269 for CP algorithm with noise $\sigma_0 = 200$, CFHB and CFRB algorithms have larger

AUC values 0.8108 and 0.7992 respectively. To improve the SNR further we considered FSI based feature measurements. Gabor, Hadamard binary and random binary features are collected directly as measurements. FHB and FRB algorithms show significant performance improvements comparing to the pixel-based feature motion detection algorithms CFHB and CFRB. However, the FG algorithm does not yield impressive performance because limited object energy is collected into feature measurement as the majority of Gabor vector elements have values close to zero. Therefore, although motion detection methods using FSI system have much better performance than using traditional system a proper choice of projection is critical to maintain a high measurement SNR. In conclusion, motion detection methods using M=1 FSI system Hadamard and random binary feature measurement present higher than 0.95 AUC values over all noise levels $\sigma_0 = 0, 20, 100,$ and 200.

For future work, we would like to consider different applications such as object motion detection and/or tracking in-vivo bio-imaging [37, 38, 39, 40]. We would also like to pursue an approach where the block size used for motion detection problem is determined adaptively based on the instantaneous needs of the imager. Here the expectation would be that the optimal block size would depend upon the spatial scale of the moving objects in a scene. In fact a spatially varying block size could further adapt to the different regions of the scene which may contain objects of different scales.

References

[1] J. Melo, A. Naftel, A. Bernardina, and J. Santos-Victor. Detection and classification of highway lanes using vehicle motion trajectories. *IEEE Transactions on Integlligent Transportation Systems*, 7:188–200, 2006.

[2] W. Hu, T. Tan, L. Wang, and S. Maybank. A survey on visual surveillance of object motion and behaviors. *IEEE Transactions on Systems, Man and Cybernetics-Part C: Applications and Reviews*, 34:334–352, 2004.

[3] E. Trucco and K. Plakas. Video tracking: A concise survey. *IEEE Journal of Oceanic Engineering*, 31:520–529, 2006.

[4] R.T. Collins, Y. Liu, and M. Leordeanu. Online selection of discriminative tracking features. *IEEE Transactions on Pattern Analysis and Machine Intelligence*, 27:1631–1643, 2005.

[5] P. Turaga, R. Chellappa, V.S. Subrahmanian, and O. Udrea. Machine recognition of human activities: A survey. *IEEE Transactions on Circuits and Systems for Video Technology*, 18:1473–1488, 2008.

[6] S.D. Blostein and H.S. Richardson. A sequential detection approach to target tracking. *IEEE Transactions on Aerospace and Electronic Systems*, 30:197–211, 1994.

[7] M.I. Skolnik. *Radar Handbook*. McGraw-Hill Professional, 1990.

[8] C. Chong, D. Garren, and T.P. Grayson. Ground target tracking - a historical perspective. *IEEE Aerospace Conference Proceedings*, pages 433–448, 2000.

[9] G. Welch and G. Bishop. An introduction to kalman filter. *Department of Computer Science, University of North Carolina at Chapel Hill*, TR 95-041, 2002.

[10] M.S. Arulampalam, S. Maskell, N. Gordon, and T. Clapp. A tutorial

on particle filters for online nonlinear/non-gaussian bayessian tracking. *IEEE Transactions on Singal Processing*, 50:174–188, 2002.

[11] A. Yilmaz, O. Javed, and M. Shah. Object tracking: A survey. *ACM Computing Surveys*, 38, 2006.

[12] R. Bartels, J. Beatty, and B. Barsky. *An Introduction to Splines for Use in Computer Graphics and Geometric Modeling*. Morgan Kaufmann, 1997.

[13] M. Kass, A. Witkin, and D. Terzopoulos. Snakes: Active contour models. *International Journal of Computer Vision*, pages 321–331, 1988.

[14] S. Zhu and C. Guo. Mathematical modeling of clutter: Descriptive vs. generative models. *Proceedings of the SPIE AeroSense Conference on Automatic Target Recognition*, 2000.

[15] S. Zhu, A. Lanterman, and M. Miller. Clutter modeling and performance analysis in automatic target recognition. *Workshop on Detection and Classification of Difficult Targets*, 1998.

[16] R.J. Radke, S. Andra, O. Al-Kofahi, and B. Roysam. Image change detection algorithms: A systematic survey. *IEEE Transactions on Image Processing*, 14:294–307, 2005.

[17] C.R. Wren, A. Azarbayejani, T. Darrell, and A.P. Pentland. Pfinder: Real-time tracking of the human body. *IEEE Transactions on Pattern Analysis and Machine Intelligence*, 19:780–785, 1997.

[18] C. Stauffer and W.E.L Grimson. Adaptive background mixture models for real-time tracking. *IEEE Computer Society Conference on. Computer Vision and Pattern Recognition*, 2:246–252, 1999.

[19] A. Elgammal, R. Duraiswami, D. Harwood, and L.S. Davis. Background and foreground modeling using nonparametric kernel density estimation for visual surveillance. *Proceedings of the IEEE*, 90:1151–1163, 2002.

[20] P. KaewTraKulPong and R. Bowden. An improved adaptive background mixture model for real-time tracking with shadow detection. *2nd European Workshop on Advanced Video Based Surveillance Systems, AVBS01*, 2001.

[21] G. Daugman. Complete discrete 2-d gabor transforms by neural networks for image analysis and compression. *IEEE Trans. on Acoustics, Speech and Signal Processing*, 36:1169–1179, 1988.

[22] Z. Sun, G. Bebis, and R. Miller. On-road vehicle detection using evolutionary gabor filter optimization. *IEEE Trans. on Intellegent Transportation Systems*, 6:125–137, 2005.

[23] T. Lee. Image representation using 2d gabor wavelets. *IEEE Trans. on Pattern Analysis and Machine Intelligence*, 18:959–971, 1996.

[24] B. Chanda and D.D. Majumder. *Digital Image Processing and Analysis.* Prentice-Hall, 2006.

[25] C. Kim and N.E. O'Connor. Using the discrete hadamard transform to detect moving objects in surveillance video. *International Conference on Computer Vision Theory and Applications*, 2009.

[26] M. Faundez-Zanuy, J. Roure, V. Espinosa-Duro, and J.A. Ortega. An efficient face verification method in a transformed domain. *Pattern Recognition Letters*, 28:854–858, 2007.

[27] Z. Liu, L. Li, Y. Song, S. Li, S. Goto, and T. Ikenaga. Motion feature and hadamard coefficient-based fast multiple reference frame motion estimation for h.264. *IEEE Trans on Circuites and Systems for Video Technology*, 18:620–632, 2008.

[28] N. Goldstein, P. Vujkovic-Cvijin, M. Fox, B. Gregor, J. Lee, J. Cline, and S. Adler-Golden. Dmd-based adaptive spectral imagers for hyperspectral imagery and direct detection of spectral signatures. *SPIE Emerging*

Digital Micromirror Device Based Systems and Applications, 7210, 2009.

[29] E.J. Candes and T. Tal. Near-optimal signal recovery from random projections: Universal encoding strategies? *IEEE Trans on Information Theory*, 52:5406–5424, 2006.

[30] J. Haupt and R. Nowak. Signal reconstruction from noisy random projections. *IEEE Trans on Information Theory*, 52:4036–4048, 2006.

[31] J. Novovicova, P. Pudil, and J. Kittler. Divergence based feature selection for multimodal class densities. *IEEE Transactions on Pattern Analysis and Machine Intelligence*, 18:218–223, 1996.

[32] http://homepages.inf.ed.ac.uk/rbf/caviardata1/.

[33] M.A. Neifeld and P. M. Shankar. Feature specific imaging. *Applied Optics*, 42:3379–3389, 2003.

[34] M.A. Neifeld and J. Ke. Optical architectures for compressive imaging. *Applied Optics*, 46:5293–5303, 2007.

[35] M.A. Neifeld, A. Ashok, and P.K. Baheti. Task-specific information for imaging system analysis. *J. Opt. Soc. Am. A*, 24:B25–B41, 2007.

[36] P. K. Baheti and M. A. Neifeld. Feature-specific structured imaging. *Applied Optics*, 45:7382–7391, 2006.

[37] E. Meijering, I. Smal, and G. Danuser. Tracking in molecular bioimaging. *IEEE signal processing magazine*, 23(3):46–53, 2006.

[38] L. Coelho, E. Glory-Afshar, J. Kangas, S. Quinn, A. Shariff, and R. Murphy. Principles of Bioimage Informatics: Focus on Machine Learning of Cell Patterns. *Linking Literature, Information, and Knowledge for Biology*, pages 8–18, 2010.

[39] S. Nie and R.N. Zare. Optical detection of single molecules. *Annual review of biophysics and biomolecular structure*, 26(1):567–596, 1997.

[40] T.W. Nattkemper. Automatic segmentation of digital micrographs: A

survey. In *Medinfo 2004: Proceedings Of THe 11th World Congress On Medical Informatics*, page 847. Ios Pr Inc, 2004.

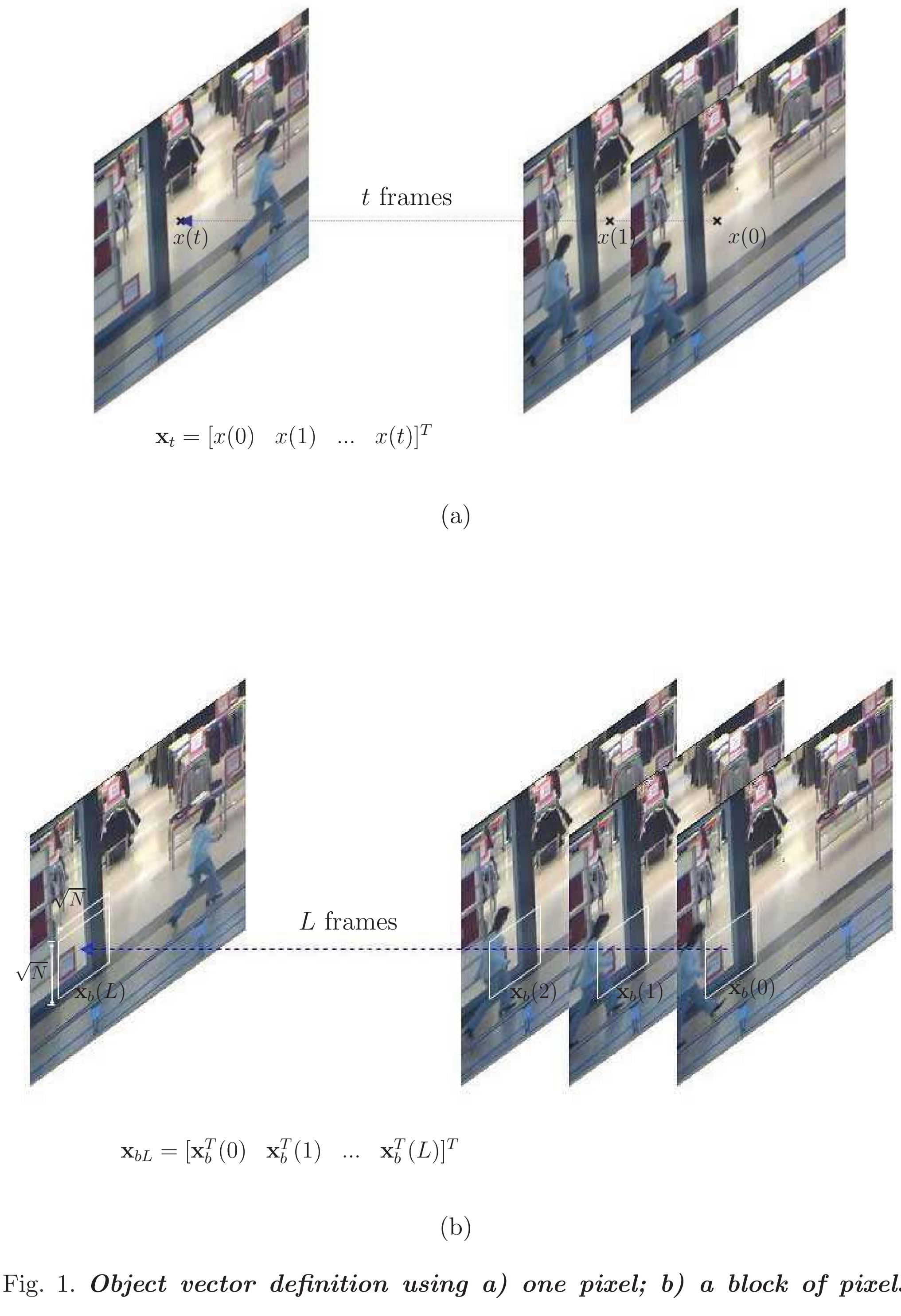

t frames
$x(t)$
$x(1)$
$x(0)$
$\mathbf{x}_t = [x(0) \quad x(1) \quad ... \quad x(t)]^T$
(a)
$\sqrt{N}$
$\sqrt{N}$
L frames
$\mathbf{x}_b(L)$
$\mathbf{x}_b(2)$
$\mathbf{x}_b(1)$
$\mathbf{x}_b(0)$
$\mathbf{x}_{bL} = [\mathbf{x}_b^T(0) \quad \mathbf{x}_b^T(1) \quad ... \quad \mathbf{x}_b^T(L)]^T$
(b)

Fig. 1. ***Object vector definition using a) one pixel; b) a block of pixels measurement.***

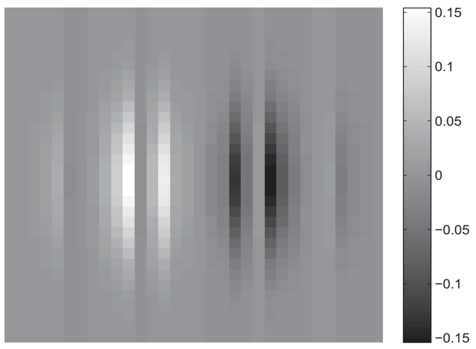

(a)

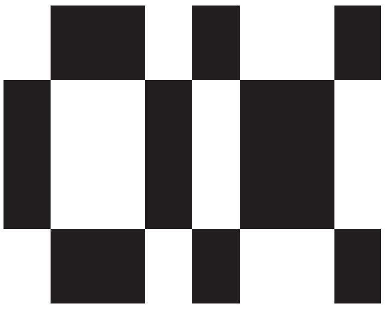

(b)

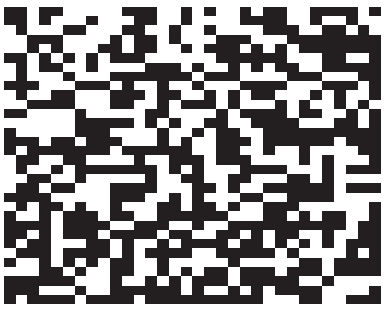

(c)

Fig. 2. Examples for a) Gabor; b) Hadamard binary; c) Random binary projections.

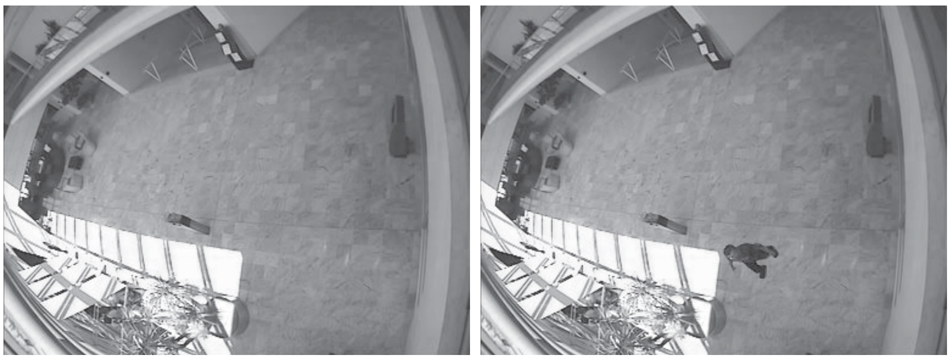

(a) (b)

Fig. 3. Examples for video frames a) without; b) with moving blocks.

Table 1

Area under ROC curves for motion detection algorithms using noiseless measurements

Algorithm	CP	CB	CDB	CFG	CFHB	CFRB
AUC	0.9985	0.9994	0.9991	0.9990	0.9994	0.9994

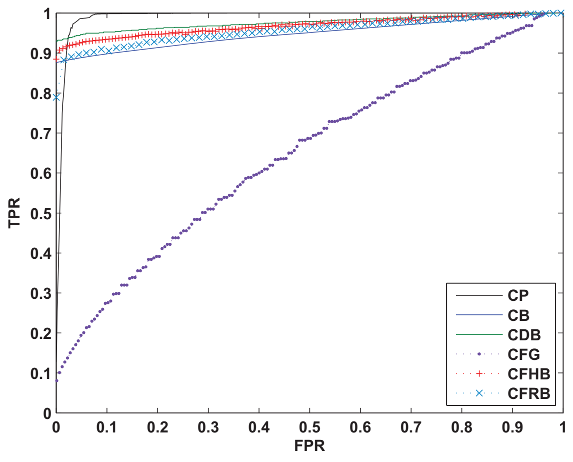

(a)

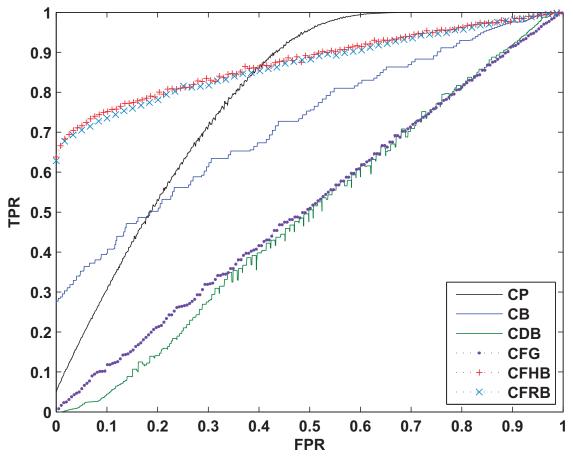

(b)

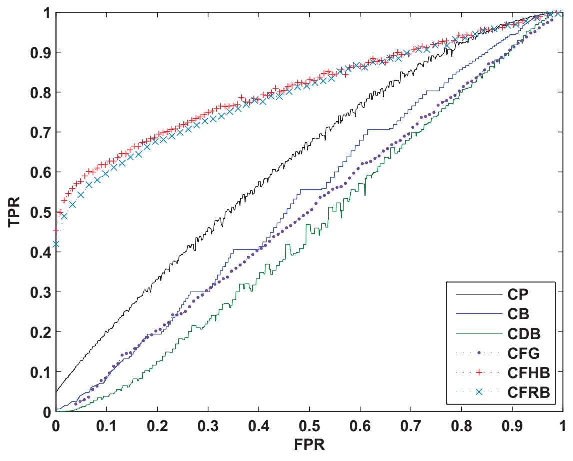

(c)

Fig. 4. ROC for algorithms using pixel-wise measurements for σ_0 is a) 20; b) 100; and c) 200.

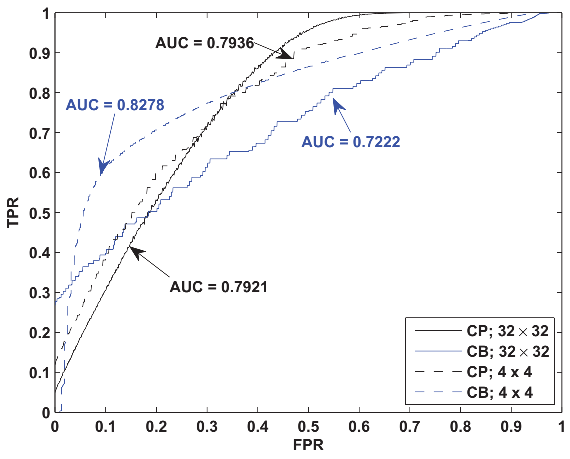

(a)

Fig. 5. ROC for CP and CB algorithms using pixel-wise measurements for $\sigma_0 = 100$ with block size 32×32 and 4×4

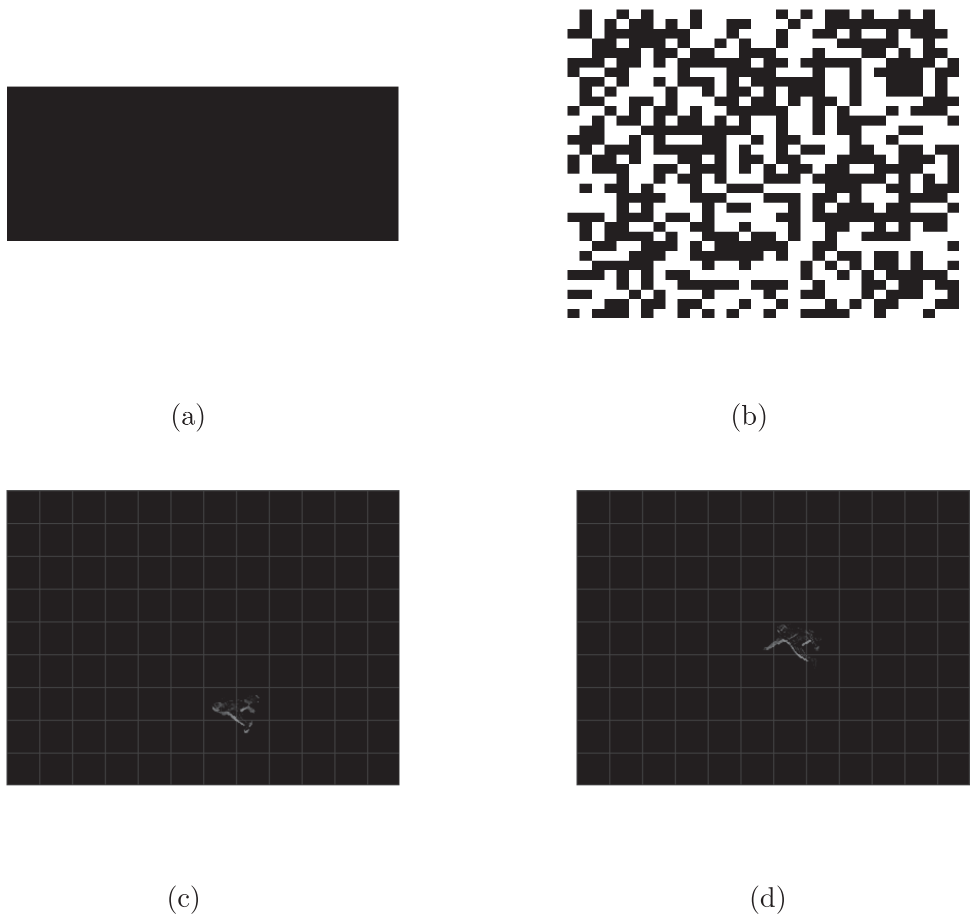

Fig. 6. The first vector in sorted a) Hadamard; b) Random binary projections; c)d) Two examples of the difference between two consecutive frames. The grid shows the blocks area in a frame.

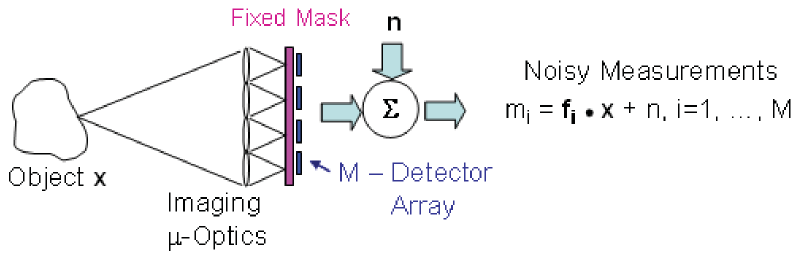

Fig. 7. FSI system with parallel architecture.

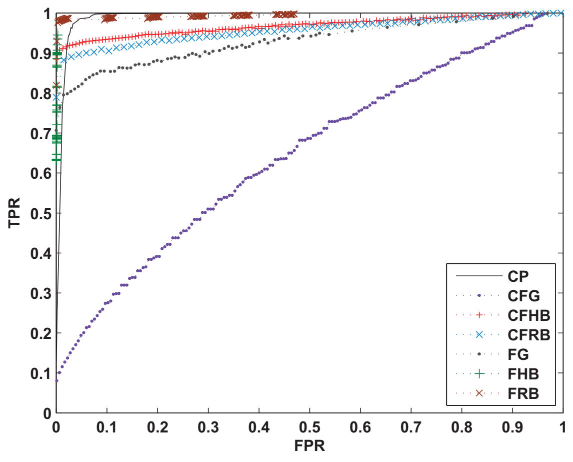

(a)

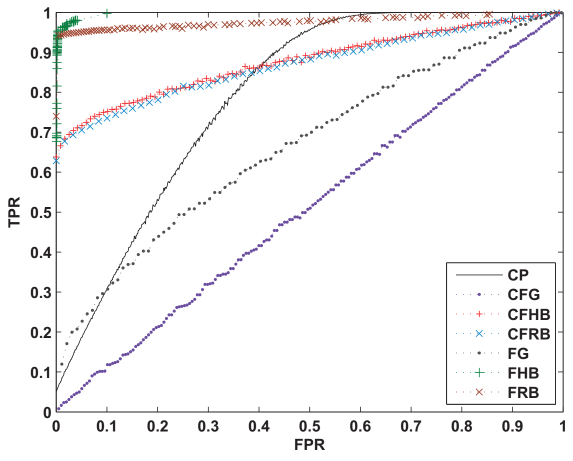

(b)

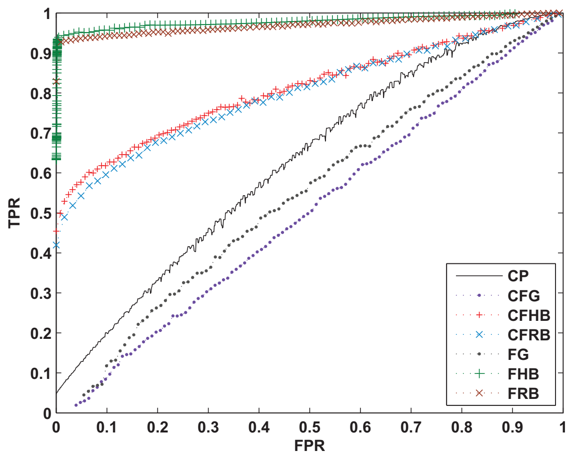

(c)

Fig. 8. ROC for algorithms using direct feature and pixel-wise measurements for σ_0 is a) 20; b) 100; and c) 200.

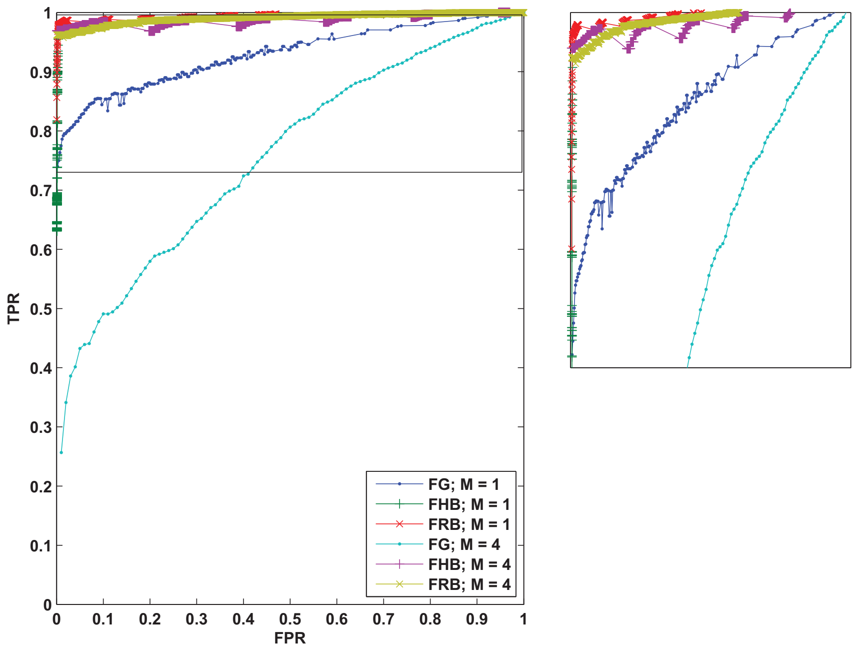
TPR
FPR
FG; M = 1
FHB; M = 1
FRB; M = 1
FG; M = 4
FHB; M = 4
FRB; M = 4

(a)

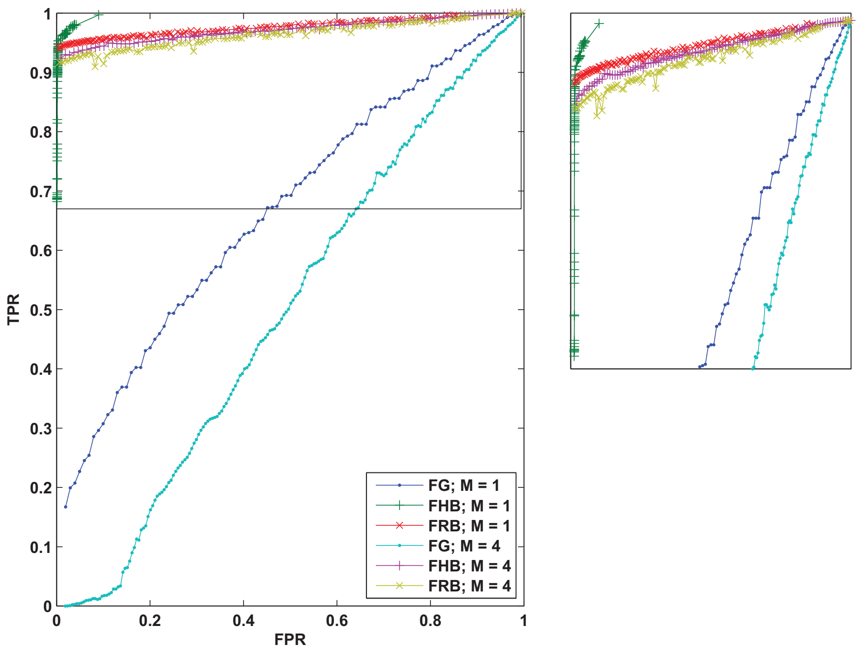
TPR
FPR
FG; M = 1
FHB; M = 1
FRB; M = 1
FG; M = 4
FHB; M = 4
FRB; M = 4

(b)

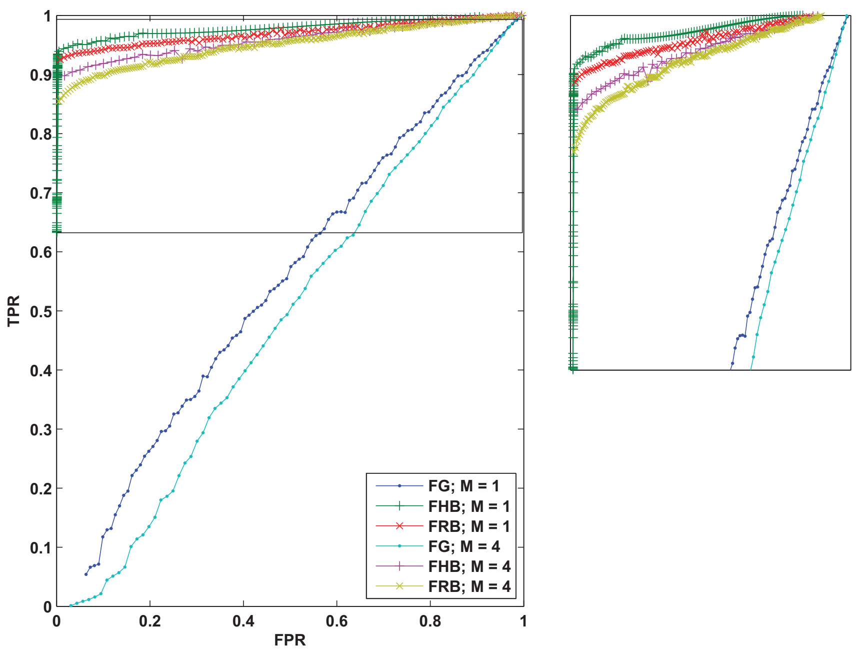

(c)

Fig. 9. ROC for algorithms using direct feature with $M = 1$ and 4 for σ_0 is a) 20; b) 100; and c) 200. The top part of each figure is magnified and presented for clarification.

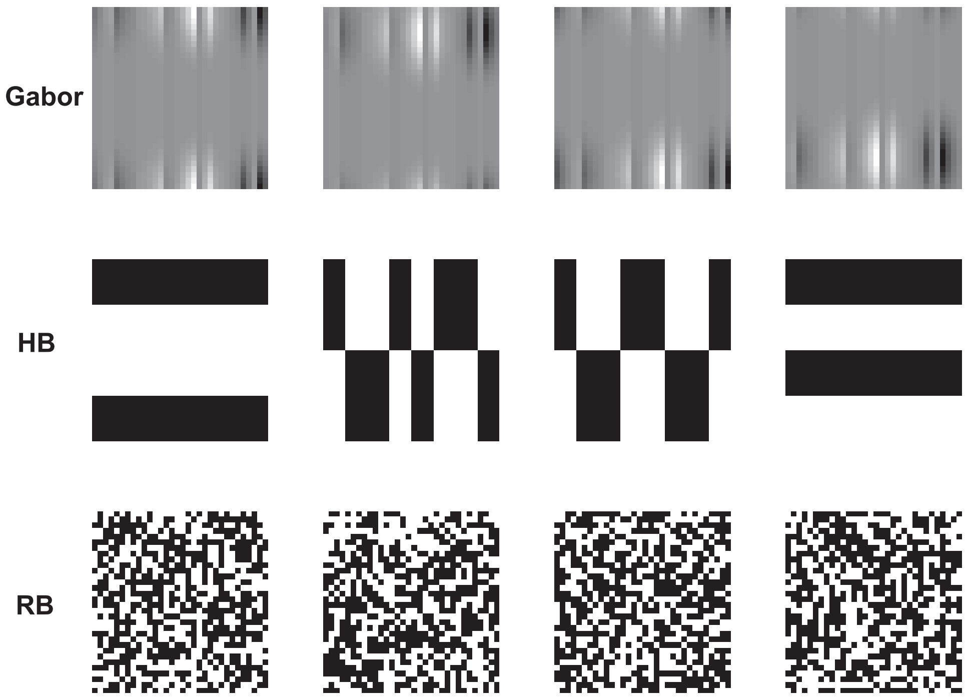

Fig. 10. The first 4 projection vectors in Gabor, Hadamard Binary, and Random Binary projections ordered from left to right with left project being the most significant.

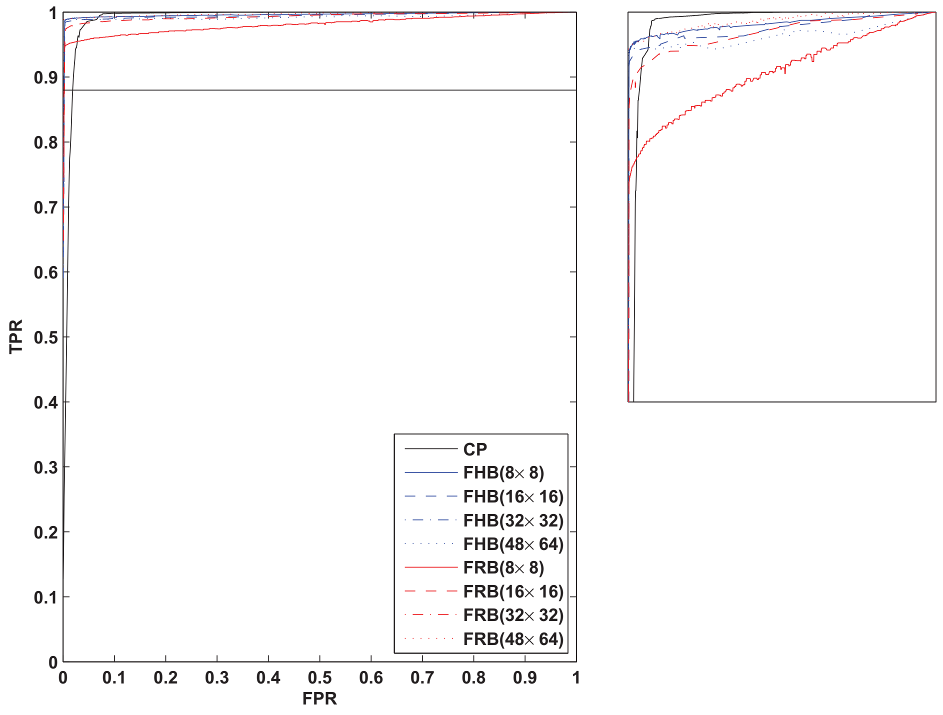

(a)

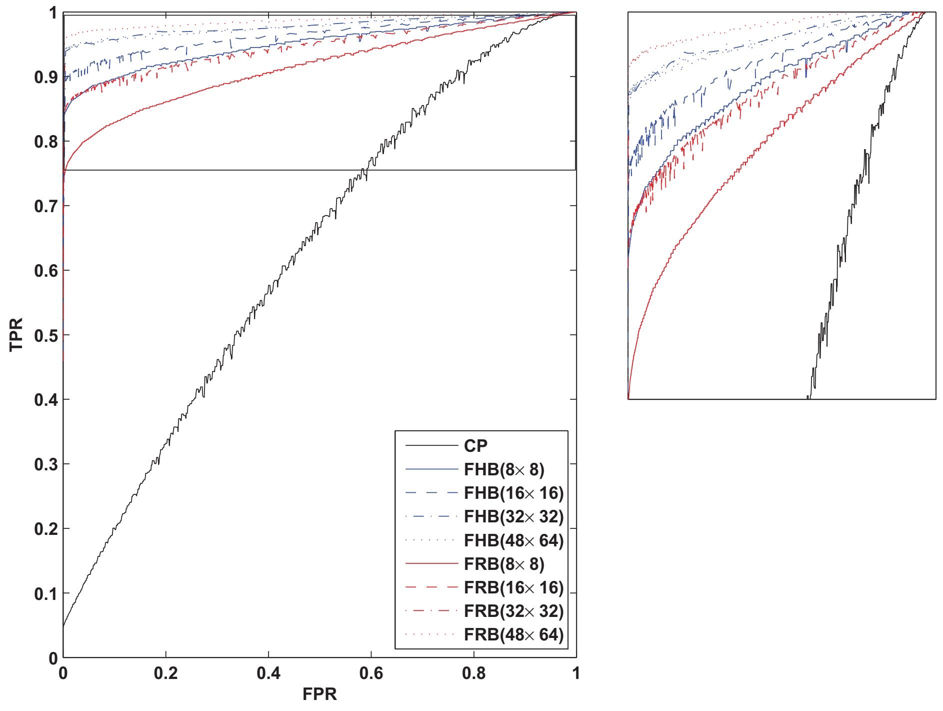

(b)

Fig. 11. ROC for CP algorithm, FHB and FRB algorithms using block size 8×8, 16×16, 32×32, and 48×64 with $M = 1$ for σ_0 is a) 20; b) 200. The top part of each figure is magnified and presented for clarification.

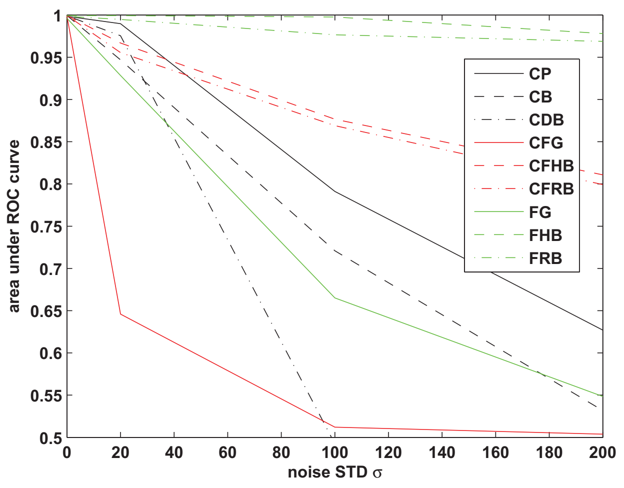

Fig. 12. Area under ROC curves for motion detection algorithms with block size 32×32.

Table 2

AUC for different detection noise σ_0 when object block size is 32×32

Algorithm	noise σ_0			
	0	20	100	200
CP	0.9985	0.9897	0.7911	0.6269
CB	0.9994	0.9468	0.7209	0.5317
CDB	0.9991	0.9755	0.4925	0.4623
CFG	0.9990	0.6458	0.5121	0.5038
CFHB	0.9994	0.9668	0.8767	0.8108
CFRB	0.9994	0.9555	0.8689	0.7992
FG	0.9961	0.9284	0.6650	0.5484
FHB	0.9993	0.9993	0.9976	0.9780
FRB	0.9985	0.9947	0.9765	0.9687

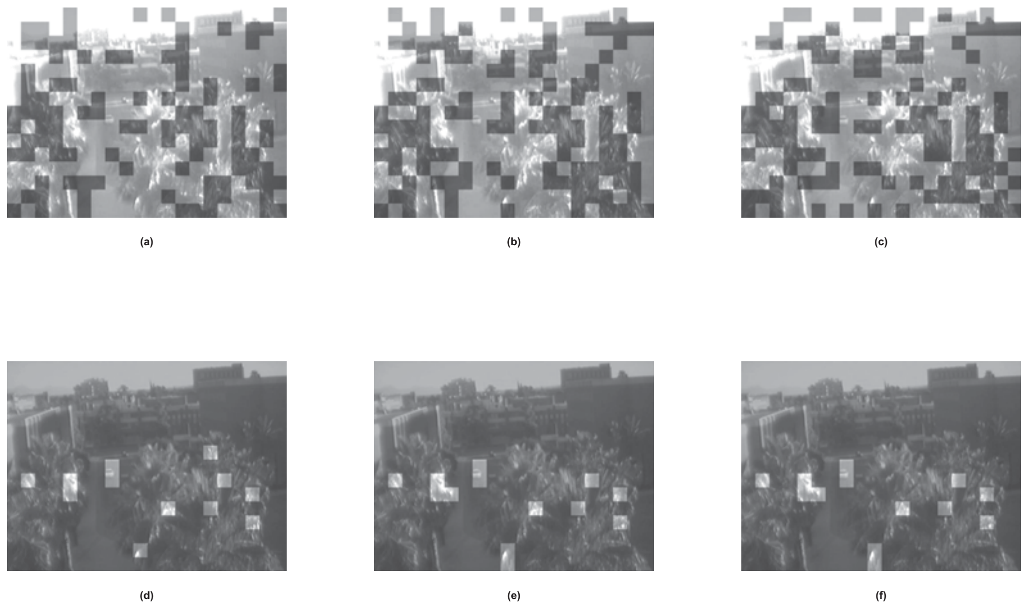

Fig. 13. Three consecutive frames with motion detected area hight lighted, using CFHB a)$\sim$c) and FHB d)$\sim$f) algorithms; noise STD - $\sigma_0 = 200$, block size - 32×32, 1 feature used for each block